Inorganic carbon assimilation by planktonic community in Santos Basin, Southwestern Atlantic Ocean

Deborah S. Kutner*[1,2], Jeff S. Bowman[2], Flávia M. P. Saldanha-Corrêa[1], Mateus G. Chuqui[1], Pedro M. Tura[1], Daniel L. Moreira[3], Frederico P. Brandini[1], Camila N. Signori[1]

[1] Universidade de São Paulo – Instituto Oceanográfico (Praça do Oceanográfico, 191 – Butantã – São Paulo – 05508-120 – SP – Brazil)
[2] University of California San Diego – Scripps Institution of Oceanography (9500 Gilman Dr, La Jolla – CA – 92093-0218 – USA)
[3] PETROBRAS Research Center – Centro de Pesquisas Leopoldo Américo Miguez de Mello (Av. Horácio de Macedo, 950 – Rio de Janeiro – 21941-915 – RJ – Brazil)

* Corresponding author: deborah.kutner@alumni.usp.br

ABSTRACT

Primary production is essential in shaping biogeochemical cycles and microbial and ecosystem dynamics. The distribution of chemosynthetic rates in pelagic zones and their participation in the carbon cycle, especially when compared to photosynthetic rates in the Southwestern Atlantic Ocean, are poorly constrained. This study aimed to measure pelagic photo- and chemosynthetic productivity and to analyze their spatial distribution and abiotic drivers. Samples for photosynthesis experiments collected at the surface and deep chlorophyll maximum (DCM) were incubated with ^{14}C-bicarbonate at eight light levels, simulating *in situ* conditions. Samples for chemosynthesis experiments were collected throughout the water column, from the surface, DCM, 250 m, 900 m, 1,200 m, and 2,300 m, and were incubated in the dark. Rates were analyzed using statistical tests to verify spatial differences between groups of samples and generalized linear models to identify correlations with environmental variables (temperature, salinity, density, mixed layer depth, dissolved oxygen, nitrite, nitrate, silicate, phosphate, turbidity, CDOM, and phycoerythrin and chlorophyll-a concentrations). Moreover, both processes were integrated from the surface to the DCM and compared at the same stations to determine the relative contribution in the epipelagic zone. The photosynthetic and chemosynthetic rates were, on average, 3.00 ± 3.26 mg C m^{-3} h^{-1} and 0.97 ± 1.22 mg C m^{-3} h^{-1}, respectively. In most stations, chemosynthesis represented an average of 10.2% of total primary productivity, but surpassed photosynthesis in three experiments (reaching 63.4 – 78.8%). Photosynthesis displayed a clear offshore-onshore gradient, along with correlated CDOM concentrations, indicating an autochthonous production of the latter. Chemosynthesis, on the other hand, exhibited high variability and lack of prediction by studied environmental variables, with isolated points of substantially higher activity.

Keywords: Primary production, Photoautotrophy, Chemoautotrophy, Carbon Cycle, Microbial dynamics

INTRODUCTION

Primary producers are essential in marine ecosystems, as their composition, biomass, and production rates shape energy and material flows through the food web and biogeochemical cycles (Kirchman, 2012). Photoautotrophs and chemoautotrophs produce organic carbon from inorganic substrates (e.g., carbon dioxide), with energy coming from sunlight and oxidation of inorganic molecules (Sorokin, 1964; Karl, 2007). Measuring these processes contributes to describing microbial dynamics and better understanding the ecosystem.

The availability of nutrients (e.g., phosphate, nitrate, ammonium, and iron) and light are the main drivers of the photosynthetic productivity of an environment. Biotic factors such as community structure (composition, physiological conditions, and abundance of organisms) and predation also determine carbon assimilation and its flow along the food web. In addition to nutrients, chemosynthetic productivity is limited by the availability of electron donors (e.g., methane, ammonium, and sulfide), which act as an energy source when oxidized (Enrich-Prast et al., 2014). Therefore, chemoautotrophs can thrive in environments with direct input of reduced compounds (e.g., oxic-anoxic interfaces in stratified water columns) or rich in organic matter, since its degradation leads to reduced compounds (electron donors).

About 1 to 40% of photosynthetic production is exported to deeper layers (Longhurst and Harrison, 1989). While sinking, part of the organic matter undergoes consumption and remineralization, hence only approximately 1% of the total produced in the euphotic zone reaches the ocean floor, which may be insufficient to sustain deep trophic chains (Herndl and Reinthaler, 2013). Recent studies on the basin adjacent to Santos, the Campos Basin, have shown that the vertical flux of particulate organic carbon is 24.2 ± 17.3 mg C m^{-2} day^{-1}, corresponding to an oligotrophic environment (Vicente et al., 2021). In this scenario, chemosynthesis may be an important source of organic carbon, especially to the deep sea; however, its contribution to the water column is still poorly understood.

Different authors have suggested the inclusion of dark carbon fixation in global carbon budgets since it can be a significant source of organic carbon. Global primary production by marine photoautotrophs is approximately 48.5 Pg C y^{-1} (Field et al., 1998). Middelburg (2011) estimated that chemoautotrophy can represent a global increment of 0.77 Pg C y^{-1} in carbon fixation (1.6% of photoautotrophy), emphasizing the contribution of nitrifiers in the euphotic zone (0.29 Pg C y^{-1}) and the dark ocean (0.11 Pg C y^{-1}). Baltar and Herndl (2019) proposed an even higher rate (1.2-11 Pg C y^{-1}), with experiments of nighttime carbon fixation increasing total primary production by 2.5-11%.

Santos Basin shelf waters are mostly oligotrophic, with low levels of chlorophyll and phytoplanktonic primary production, due to the presence of the Tropical Water (TW), brought by the Brazil Current (Gaeta and Brandini, 2006; Lutz et al., 2018). However, inner shelf areas display mesotrophic conditions due to continental runoff (Coastal Water, CW) and eutrophic conditions as a result of anthropic pressure, such as the Santos and Guanabara bays (Aidar-Aragão et al., 1980; Aguiar et al., 2011). The Cabo Frio region also stands out, with high chlorophyll concentrations and primary production rates in the productive phase of the upwelling of the nutrient-rich South Atlantic Central Water (Gonzalez-Rodriguez et al., 1992). On the other hand, the phytoplankton community in upper layers is mainly dominated by the pico- (0.2–2 µm) and nanoplanktonic (2–20 µm) size-fractions, which is characteristic of an oligotrophic environment (Brandini et al., 2014; Bergo et al., 2017). This has direct implications in shaping colored dissolved organic matter (CDOM) temporal dynamics, as it is an essential product of phytoplankton metabolism and greatly depends on the abundance of picophytoplankton (Organelli and Claustre, 2019). At the deep chlorophyll maximum (DCM) layer, there is a greater contribution of microplankton (20-200 µm), mainly composed by diatoms along the thermocline (Brandini et al., 2014).

The magnitude and distribution of primary production have been reported in previous studies in the Santos Basin (Gaeta and Brandini, 2006; Brandini, 1990a). However, estimates of carbon assimilation contribution by chemosynthetic processes simultaneously with photosynthesis measurements, on a broader scale, have not been carried out as a way of evaluating the contribution of both processes to the synthesis of organic carbon in the pelagic environment. Furthermore, the Santos Basin is characterized by different biogeochemical fronts driven by physical mechanisms (Brandini et al., 2018), making it a remarkable region for exploring spatial patterns and relations between productivity and environmental parameters. Generalized linear models (GLMs), an advance in regression analysis, are convenient for assessing these relationships. GLMs are useful

tools when handling normal (Gaussian) and non-normal (e.g. binomial, Poisson, etc.) distributions and work well with classical statistical practices in linear modeling and analysis of variance (Guisan et al., 2002). Moreover, GLMs use a consistent scale of measurement (the same as the response variable), allowing for straightforward model comparisons (Crawley, 2015).

Therefore, this study aimed to assess the relative importance of photo- and chemosynthesis to total primary productivity in the Santos Basin. The two processes were compared in the epipelagic zone and the analysis of chemosynthesis extended throughout the whole water column. Furthermore, we used GLMs to elucidate abiotic drivers for each carbon assimilation process.

METHODS

Study area

Santos Basin (Figure 1) comprises an area of approximately 350,000 km^2 of the southern Brazilian continental margin. The basin is bounded by Cabo Frio High to the north (23°S), Florianópolis High to the south (28°S), and the São Paulo plateau follows the basin in structural and stratigraphic continuity to the east (Moreira et al., 2007). The continental

shelf extends to a depth of 200 m, followed by the continental slope to a depth of 2,000 m and the open ocean to a depth of 3,000 m.

The hydrographic structure is characterized by the presence of the following water masses: Tropical Water (TW), South Atlantic Coastal Water (SACW), Antarctic Intermediate Water (AAIW), Upper Circumpolar Deep Water (UCDW), North Atlantic Deep Water (NADW), Lower Circumpolar Deep Water (LCDW), and Antarctic Bottom Water (AABW). Water mass ranges defined by Silveira et al. (2023) were used. The Brazil Current flows southwards along the shelf break, working as a boundary, while the Intermediate Western Boundary Current flows equatorward in intermediate layers. The interface between these currents and the bathymetry of the region favor physical features with biogeochemical consequences, such as eddies, meanders, and upwellings (Silveira et al., 2020). Coastal Water (CW) was used to identify warmer and less saline waters (compared to the TW) on the continental shelf, influenced by the TW, SACW, and river runoff (Castro, 2014). Mixed Water (MW) denotes waters without clear temperature-salinity identity (composition of less than 55% of a specific water mass (Dottori et al., 2023)).
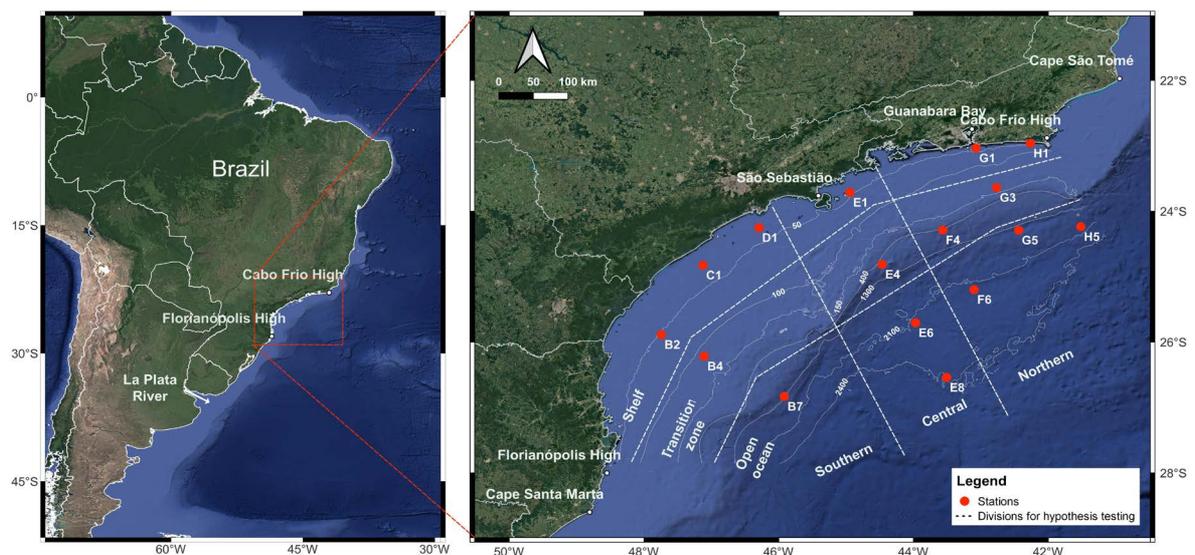

Figure 1. Santos Basin with key features, oceanographic stations (red filled circles) and groups of samples for hypothesis testing: distance from coastline (shelf, transition zone, and open ocean) and groups of transects (southern, central, and northern regions).

SAMPLING STRATEGY

Within the scope of the Santos Project – Regional Environmental Characterization of Santos Basin, coordinated by Petrobras, samples were collected between August and October 2019 aboard the R/V *Ocean Stalwart*. Experiments of photo- and chemosynthetic production were carried out at 15 and 16 oceanographic stations, respectively (Figure 1). Although environmental parameters (temperature, salinity, neutral density, mixed layer depth, dissolved oxygen, nitrite, nitrate, silicate, phosphate, turbidity, colored dissolved organic matter (CDOM), and phycoerythrin and chlorophyll-a concentration) were sampled across 60 stations, only data corresponding to the same 16 experiments were analyzed in this study (the complete sampling map is present in Moreira et al., 2023). Seawater and physical data were collected at six depths (surface, deep chlorophyll maximum (DCM), 250 m, 900 m, 1,200 m, and 2,300 m) using a combined Sea-Bird Electronics CTD (model SBE 9plus)/Carrousel 911 system equipped with 24 Niskin bottles (10 L). Depths were chosen for sampling the different water masses present in the region. The DCM at each station was identified by the profile of fluorescence given by the CTD (Moreira et al., 2023).

ENVIRONMENTAL PARAMETERS

The CTD was equipped with sensors of conductivity, temperature, depth (pressure), dissolved oxygen, turbidity, CDOM, chlorophyll-a, and phycoerythrin. The profiles of conductivity, temperature, pressure, and turbidity were processed and reviewed by the Ocean Dynamics Laboratory and the Coastal Hydrodynamics Lab at the Oceanographic Institute of University of São Paulo (IOUSP). CTD downcast data were spike-removed, averaged into a 1 m bin, and smoothed, as reported by Silveira et al. (2023). Temperature, salinity, and density (derived from the prior two) were adjusted to conservative temperature, absolute salinity, and neutral density according to the Thermodynamic Equation of Seawater of 2010 (IOC et al., 2010). Mixed layer depth (MLD) for the continental shelf (< 200 m deep) was considered as the minimum depth between vertical Laplacian values of conservative

temperature (> 0.225°C m^{-2}), practical salinity (> 0.00625 PSU m^{-2}), and neutral density (> 0.025 (kg m^{-3}) m^{-2}). In oceanic regions (> 200 m deep), MLD was determined by the depth at which neutral density was higher than 0.125 kg m^{-3}.

Dissolved oxygen, CDOM, chlorophyll-a, and turbidity sensors were calibrated according to manufacturer recommendations, and corrections were performed by the Marine Biogeochemistry Laboratory (LABMAR) at IOUSP. For dissolved oxygen (more information on the sensor is present at https://www.seabird.com/asset-get.download.jsa?id=54627861704), corrections were made by linear regressions between CTD and Winkler analysis results (Grasshoff et al., 2009). To correct chlorophyll-a concentrations, the same method was applied between CTD and fluorimetry results from water samples (according to Welschmeyer, 1994). For CDOM and turbidity, corrections were performed using quinine sulfate dilutions of 0.5, 1.0, 2.5, 5.0, 10.0, and 25.0 ppb QSU and Formazin dilutions of 0.5, 1.0, 2.5, 5.0, 7.5, and 10 NTU, respectively (more information on the calibration of sensors is present at http://docs.turnerdesigns.com/t2/doc/appnotes/S-0081.pdf). The phycoerythrin sensor was not calibrated, hence the raw data are provided in volts (Table S1). Concentrations of inorganic nutrients (nitrate, nitrite, phosphate, and silicate) were determined using a flow injection autoanalyzer (SEAL Analytical AutoAnalyzer III), according to Grasshoff et al. (2009). All nutrients were collected and analyzed by the LABMAR team.

EXPERIMENTS OF PHOTOSYNTHESIS AND CHEMOSYNTHESIS

We refer to photosynthesis as the estimation of dissolved inorganic carbon (DIC) fixation under light conditions subtracting dark carbon fixation. Rates were measured according to the *in situ* simulated method with ^{14}C-bicarbonate developed by Steemann-Nielsen (1952). Photosynthesis–Irradiance curves (P-I curves) were conducted with one surface and one DCM sample for eight sunlight levels at the surface (100%, 55%, 37%, 16%, 8%, 4%, 1%, and 0% as the "blank"). They were incubated in 70 mL borosilicate flasks with 5 µCi of ^{14}C-bicarbonate for between 5-8 h.

Experiments were conducted in open incubator chambers on the ship deck, starting between 08 am and 11 am to ensure sunlight. Temperature was maintained by surface seawater circulation around the system.

To create different light levels, combinations of blue correction lighting filters that simulate seawater irradiance attenuation (Roscolux, Cinegel, R3206 Third Blue CTB) and light and dark grey filters were used to reduce intensity without affecting color temperature (Roscolux, Cinegel R97 Light Grey and Cinegel R3415 Rosco N.15). The light intensity inside each one was measured with the Quantum Scalar Irradiance Meter QSL-100 by Biospherical Instruments.

Chemosynthesis, also referred to as dark carbon fixation, was considered organic matter production without the use of sunlight energy. Rates were measured according to an adapted version of the ^{14}C-bicarbonate method developed by Steemann-Nielsen (1952), which has been used elsewhere (e. g., Casamayor et al., 2008; Reinthaler et al., 2010; Signori et al., 2018). Experiments were conducted for the six sampling depths. For each one, three flasks (one blank and two replicates) with 70 mL of seawater were incubated with 5 µCi of ^{14}C-bicarbonate for 9-12 h in the dark. A 2% formaldehyde solution was added to the blank flask to terminate biological activity before incubation. Surface and DCM samples were incubated at room temperature (ca. 22°C). Samples collected at 250 m were incubated under air conditioning (ca. 17°C) and samples collected at and below 900 m were incubated in a refrigerator (ca. 4°C), to best simulate *in situ* temperature conditions.

After the incubations, samples of photo- and chemosynthesis were filtered onto 0.22 µm polycarbonate membranes (Millipore, MA) using a vacuum pump and manifold. At the Multiuser Radioisotope Laboratory (IOUSP), membranes were exposed to concentrated HCl fumes for 30 s to remove remaining $^{14}CO_2$, placed in scintillation vials with 5 mL of liquid scintillation cocktail (Ultima Gold, PerkinElmer), and left in the dark for at least 24 h. Each sample was analyzed for 30 min in a scintillation spectrometer (PerkinElmer Tricarb 2810 TR), and the resulting disintegrations per

minute (DPM) were converted into production (P) rates of carbon per volume and time according to Teixeira (1973):

$$P\left(mgCL^{-1}h^{-1}\right) = \frac{DPM_{sample}}{DPM_{available}} \times \frac{1}{T} \times \left[CO_2\right] \times \frac{12}{44} \times K_{1,2} \quad (1)$$

where the fraction of assimilated DPM is multiplied by 1.06 (correction factor for isotopic ratio), T is incubation time (h), $[CO_2]$ × 12/44 is the C concentration from CO_2 in the water (mg L^{-1}), K_1 is the relative correction factor for the sample volume (in case the incubated and filtered volumes are different), and K_2 is the dimensional factor to convert to other units. Moreover, $[CO_2]$ = 90 mg L^{-1} (Steemann-Nielsen, 1952) and K_2 = 1,000 were used to convert to mg C m^{-3} h^{-1}.

To obtain the photosynthetic rate for each sampling depth, P-I curves were plotted for the surface and for the DCM in Kaleidagraph version 4.0 (Synergy Software). The empirical and continuous function described by Platt et al. (1980) was used to adjust the curve fit without biomass normalization to allow for comparisons with chemosynthetic rates (that were not normalized):

$$P = P_s\left(1 - e^{\left(\frac{-\alpha I_d}{P_s}\right)}\right)e^{\left(\frac{-\beta I_d}{P_s}\right)} \quad (2)$$

where P (in mg C m^{-3} h^{-1}) is the productivity given a downward irradiance I_d (in µmol photons m^{2} s^{1}), P_s (in mg C m^{-3} h^{-1}) is the maximum photosynthetic rate the sample could sustain if there were no photoinhibition (a parameter that can be derived to obtain Pm, the maximum productivity at optimal light intensity), α (in mg C m^{-3} h^{-1} (µmol photons m^{-2} s^{-1}) $^{-1}$) is the initial slope of the curve, and β (in mg C m^{-3} h^{-1} (µmol photons m^{2} s^{-1}) $^{-1}$) is the photoinhibition parameter.

The irradiance values for the curve were obtained from the clear sky model for direct and diffuse insolation by Bird and Hulstrom (1981). Morel's (1991) definition of photosynthetically active radiation (PAR, in mol photons m^{-2}) just above ocean surface (z = 0) was used, which is the double integral of downward irradiance at the surface ($I_{d\ (z=0)}$) given a range of wavelengths λ

(usually λ_1 = 400 nm; λ_2 = 700 nm) and time t (from 0 to daylength L):

$$PAR\left(0^+\right) = \int_0^L \int_{\lambda_1}^{\lambda_2} I_d\left(\lambda, 0^+, t\right) d\lambda \, dt \qquad (3)$$

To select the range between 400 and 700 nm of the results of the irradiance model, which are already integrated in the whole spectral domain, they were multiplied by 0.48 (Frouin and Pinker, 1995). Then, they were multiplied by 4.57 to convert units from W m^{-2} to µmol photons m^{-2} s^{-1} (Thimijan and Heins, 1983) and integrated during the incubation period (from t_0 to t, in s) using the trapezoid method in Python 3.8.2 (2020). Finally, results were divided by the total incubation time (T, in s) to obtain an average irradiance (in µmol photons m^{-2} s^{-1}) at the surface during the experiment, which was used as the 100% value in the P-I curve:

$$I_{d(z=0)} = \frac{1}{T} \int_{t_0}^{t} I_d(t) \times 0.48 \times 4.57 \, dt \qquad (4)$$

To obtain the irradiances in the curve, $I_{d(z=0)}$ was multiplied by the percentage of light attenuation in the incubation bottle. Once the P-I curves were adjusted for each depth in each station, the percentage of light in each sampling depth (Kirk, 2011), given by the Secchi depth (Poole and Atkins, 1929), was used to select the corresponding photosynthetic rate in the P-I curve:

$$I_d(z) = I_d(0) \times e^{-K_d z} \qquad (5)$$

where $I_d(z)$ and $I_d(0)$ are, respectively, the downward irradiances in µmol photons m^{-2} s^{-1} at z m depth and at the surface, and K_d is the mean vertical attenuation coefficient from 0 to z m, which was estimated by dividing 1.7 by the Secchi depth (Poole and Atkins, 1929).

Photo- and chemosynthetic rates were integrated from surface to DCM by the trapezoidal method and the results in mg C m^{-2} h^{-1} represent the relative contribution of each process in the epipelagic zone.

Data analysis

Data were analyzed and visualized using RStudio® version 4.1.2 (R Core Team, 2021),

Ocean Data View (ODV) version 5.5.2 (Schlitzer, 2021), and QGIS version 3.22.6 (2022).

Photo- and chemosynthesis rates were analyzed using statistical tests to verify spatial differences between means of samples when considering different groups of transects across the basin (northern, central, and southern) and the distance from the coastline (shelf, transition zone, and open ocean) (Figure 1). Different water masses present in the region and depths – surface and DCM layers for photosynthesis; epi- (0 – 200 m; encompassing surface and DCM samples), meso- (200 – 1,000 m; encompassing 250 and 1,200 m samples), and bathypelagic (1,000 – 4,000 m; encompassing 1,200 and 2,300 m samples) zones for chemosynthesis – were also tested for significant differences. The Levene's test, from the "car" package in RStudio® (Fox and Weisberg, 2019), was used to test the homogeneity of variances between groups of samples, and the Shapiro-Wilk test was conducted to evaluate the normality of residuals. Statistical significance was considered when p-value < 0.05. Since data did not fit the assumption of normality, log(x) and sqrt(x) transformations were applied to photosynthetic and chemosynthetic rates, respectively. Extreme outliers, defined as higher than the third quartile plus three times the interquartile range, were excluded from statistical analyses. Statistical differences between three groups were evaluated by a two-way Analysis of Variance (ANOVA) and between two groups by a two-way Student's t-test. Each was followed by a Tukey's Honest Significant Difference (HSD) test to identify possible differences. The results were represented with boxplots, from the "ggplot2" package in RStudio® (Wickham, 2016), with individual observations (including outliers) plotted as points and whiskers extending to 1.5 times the interquartile range of the sample.

Because temperature can affect microbial metabolic processes (López-Urrutia et al., 2006; Regaudie-de-Gioux and Duarte, 2012; Bergo et al., 2017; Frazão et al., 2021), a possible increase in DCM productivity rates was estimated due to incubation of DCM samples at surface temperature. The temperature coefficient (Q_{10}) given by Van 't Hoff's equation represents

the increase in a certain reaction rate when temperature is raised by 10 K:

$$\frac{R_2}{R_1} = Q_{10}^{\frac{T_2 - T_1}{10}} \quad (6)$$

where R_1 and R_2 are the reaction rates at temperatures T_1 and T_2, respectively. To estimate a mean ratio between R_2 (measured rates) and R_1 (possible DCM rates due to difference in temperature), T_1 was considered equal to average DCM *in situ* temperature and T_2 to the incubation temperature of DCM samples (average surface water temperature for photosynthesis and approximate room temperature for chemosynthesis). The calculations were made separately for photo- and chemosynthesis, but with $Q_{10} = 2.04$ (specific log normalized gross primary production relative to chlorophyll-a value for the Atlantic Ocean, given by Regaudie-de-Gioux and Duarte (2012) for both processes, since a specific value for the latter was not found in the literature. Initial rates were then divided by the R_2/R_1 ratio, considering their increase by temperature difference, and normalized by the same transformations. A two-way Student's t-test was applied to compare normalized initial and final rates and check if the simulated values of productivity were significantly different from the measured rates.

To analyze the influence of abiotic factors, the productivity rates were plotted over a Non-Metric Multidimensional Scaling (nMDS) ordination. The variables used on the nMDS with Bray-Curtis dissimilarity metric were conservative temperature, absolute salinity, depth, mixed layer depth, dissolved oxygen, nitrite, nitrate, silicate, phosphate, turbidity, CDOM, and chlorophyll-a and phycoerythrin concentrations. To validate nMDS results, a Permutational Multivariate Analysis of Variance (PERMANOVA) was carried out for the following groups of samples: distance from coastline, depth layers, pelagic zones, water masses, and groups of transects, as previously described. Both analyses were conducted with the "vegan" package in RStudio® (Oksanen et al., 2020).

To assess the power of the variables in predicting photo- and chemosynthesis, generalized linear models were used according to Bowman et al. (2018). A null model was created with the productivity

rates as the response variable and the following explanatory variables: conservative temperature, absolute salinity, neutral density, mixed layer depth, dissolved oxygen, nitrite, nitrate, silicate, phosphate, turbidity, CDOM, and chlorophyll-a and phycoerythrin concentrations. Possible models were built by the stepwise addition of predictors given the significance of the difference between their slope and 0 in a Student's t-test. Each model was tested for multiple collinearities between variables by the calculation of variance inflation factors (VIF) by the "VIF" command from the "car" package in RStudio® (Fox and Weisberg, 2019). Models containing predictors with VIF > 5 were discarded to avoid overfitting, and the variable that caused multicollinearity was excluded from other possible models. After calculating the Akaike's Information Criterion (AIC) for each model, the best model (lowest AIC) was compared to the others by relative likelihood and they were discarded if the value was < 0.05. Finally, the model with fewest parameters was evaluated against the remaining possibilities by ANOVA and the chi-squared test and was selected as the winning model when not significantly different from the others ($p > 0.05$).

The winning model was validated by a bootstrap approach. A set of 1,000 models were built from random subsets of observations, each time retaining three out of the total number of observations (28 for photosynthesis and 54 for chemosynthesis) to include as much training data as possible. Each model had to predict the process for the three observations that were not included in the training set. The predicted response was plotted as a function of the observed response, with the standard deviation of each point across all the iterations.

RESULTS

Photosynthetic rates varied from 0.48 to 13.47 mg C m^{-3} h^{-1} (except for the extreme outlier of station G1, equal to 62.98 mg C m^{-3} h^{-1} – surface waters in front of the Guanabara Bay), with mean and standard deviation equal to 3.00 ± 3.26 mg C m^{-3} h^{-1}. Differences across the transects and layers were insignificant (ANOVA, $p = 0.79$, and Student's t-test, $p = 0.46$, respectively) (Figures 2B and 2C). An offshore-onshore gradient (ANOVA, $p < 0.001$) was detected, with higher productivity on the shelf (Tukey HSD test), where the mean

was 5.91 mg C m^{-3} h^{-1}. Means in the transition zone and open ocean were, respectively, 1.26 and 1.02 mg C m^{-3} h^{-1} (Figure 2A). This pattern of variation was also confirmed by the significant difference between water masses (ANOVA, $p < 0.001$). The higher photosynthetic rates

were in the Coastal and Mixed Water, and the lower in the Tropical Water (Table 1, Figure S1A). Since the Tukey HSD test showed no difference between rates in the CW and MW, they were considered in the same group in further interpretations.

Table 1. Conservative temperature (°C), absolute salinity, photosynthesis (mg C m^{-3} h^{-1}) and chemosynthesis (mg C m^{-3} h^{-1}) statistics (mean values, SD = standard deviations, median values, range from minimum to maximum and N = number of observations) for all stations according to water masses: Coastal Water (CW), Tropical Water (TW), Mixed Water (MW), South Atlantic Central Water (SACW), Antarctic Intermediate Water (AAIW), Upper Circumpolar Deep Water (UCDW), North Atlantic Deep Water (NADW).

Parameter	Statistic	CW	TW	MW	SACW	AAIW	UCDW	NADW
Conservative temperature (°C)	Mean ± SD	19.6 ± 1.3	21.9 ± 1.1	21.1 ± 2.8	15.7 ± 1.8	4.4 ± 0.35	3.4 ± 0.1	3.4 ± 0.1
	Median	19.8	21.9	23.1	15.7	4.4	3.4	3.4
	Range	17.6 – 21.5	19.3 – 23.6	18.0 – 23.2	13.2 – 17.7	3.9 – 4.8	3.3 – 3.5	3.3 – 3.4
	N	8	21	5	8	7	4	2
Absolute salinity	Mean ± SD	33.7 ± 0.6	36.8 ± 0.5	35.4 ± 0.6	35.8 ± 0.3	34.5 ± 0.02	34.7 ± 0.02	35.1 ± 0.01
	Median	33.7	36.9	35.2	35.8	34.5	34.7	35.1
	Range	32.8 – 34.5	35.7 – 37.3	34.8 – 36.0	35.4 – 36.1	34.5 – 34.5	34.6 – 34.7	35.1 – 35.1
	N	8	21	5	8	7	4	2
Photosynthesis (mg C m^{-3} h^{-1})	Mean ± SD	3.9 ± 2.0	1.8 ± 3.0	8.07 ± 2.4[1]	-	-	-	-
	Median	4.1	1.0	6.8[1]	-	-	-	-
	Range	1.2 – 7.7	0.5 – 13.5	6.6 – 10.8[1]	-	-	-	-
	N	7	18	3[1]	-	-	-	-
Chemosynthesis (mg C m^{-3} h^{-1})	Mean ± SD	0.2 ± 0.4	1.3 ± 1.5	0.9 ± 0.6	1.0 ± 1.3	1.0 ± 0.9	1.2 ± 1.9	0.6 ± 0.8
	Median	0.04	0.5	0.8	0.4	1.1	0.4	0.6
	Range	0.03 – 1.1	0.002 – 4.47	0.3 – 1.9	0.02 – 3.6	0.002 – 2.3	0.002 – 4.1	0.02 – 1.1
	N	8	20	5	8	7	4	2

[1]Extreme outlier (station G1 – surface) was removed.

Chemosynthetic rates varied from 0.002 to 4.47 mg C m^{-3} h^{-1}, with mean and standard deviation equal to 0.97 ± 1.22 mg C m^{-3} h^{-1}. Even after sqrt(x) transformation, p-values from Shapiro-Wilk were close to, but not smaller than, 0.05. Thus, we chose to continue with the parametric test ANOVA given its robustness. Differences in groups by ANOVA tests were only significant ($p < 0.001$) for northern, central, and southern regions of the basin, with all means different (Tukey HSD test), respectively 0.51, 2.25, and 0.03 mg C m^{-3} h^{-1} (Figure 2E). We found no significant differences with increasing distance from the coastline (Figure 2D), between pelagic zones (Figure 2F), and water masses (ANOVA, $p = 0.23, 0.96$, and 0.44, respectively). Although chemosynthesis is apparently higher on the TW

compared to the CW by looking at its mean in each water mass (respectively 1.3 and 0.2 mg C m^{-3} h^{-1}; Table 1) and at the temperature-salinity space (Figure S1B), we observed no significant pattern, as water mass analysis showed.

When comparing the two processes, chemosynthesis was responsible for, on average, 24.3% of the total integrated DIC fixation from surface to DCM (Figure 3). In stations where it was lower than photosynthesis, chemosynthesis represented, on average, 10.2% of the total primary productivity or 14.6% of photosynthesis. However, chemosynthetic rates were higher than photosynthetic rates at three stations (E4, E6, and H5), making up 63.4% to 78.8% of total productivity in offshore waters.
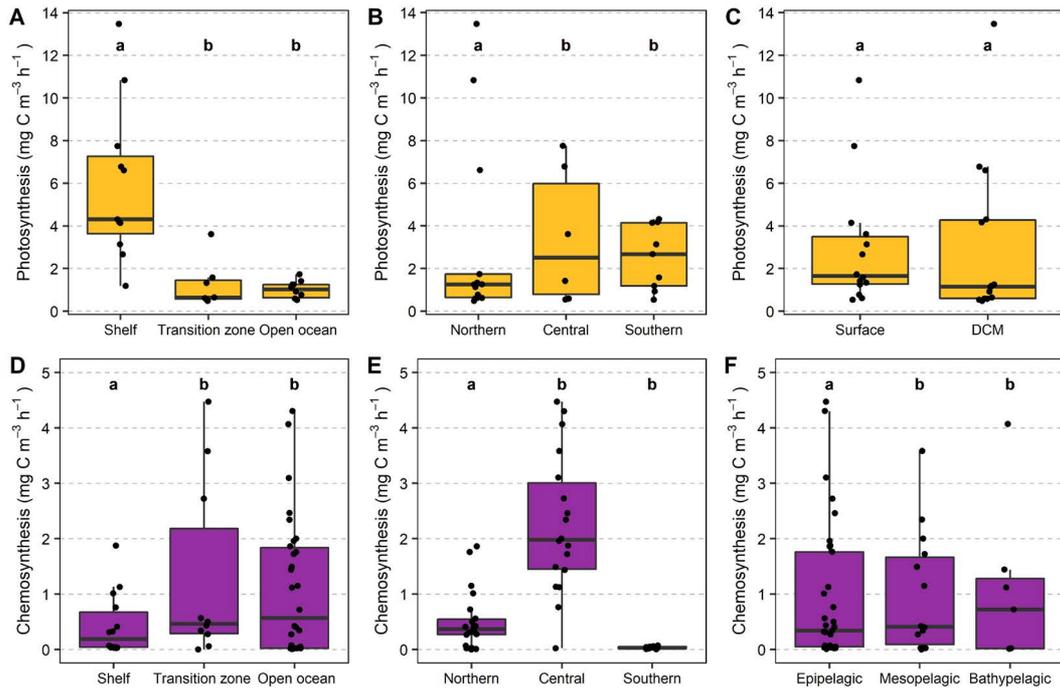
Figure 2. Spatial distribution of photo- (A, B, C) and chemosynthetic (D, E, F) rates. Variability of each rate is presented for distance from coastline (A, D), groups of transects (B, E) and vertical layers: surface and deep chlorophyll maximum (DCM) (C) or pelagic zones (F). Significance was tested within each group by ANOVA tests ($p < 0.05$). Different letters (a, b, c) indicate significant differences; same letters indicate no significant difference. Points represent observations and whiskers extend to 1.5 times the interquartile range of the sample.
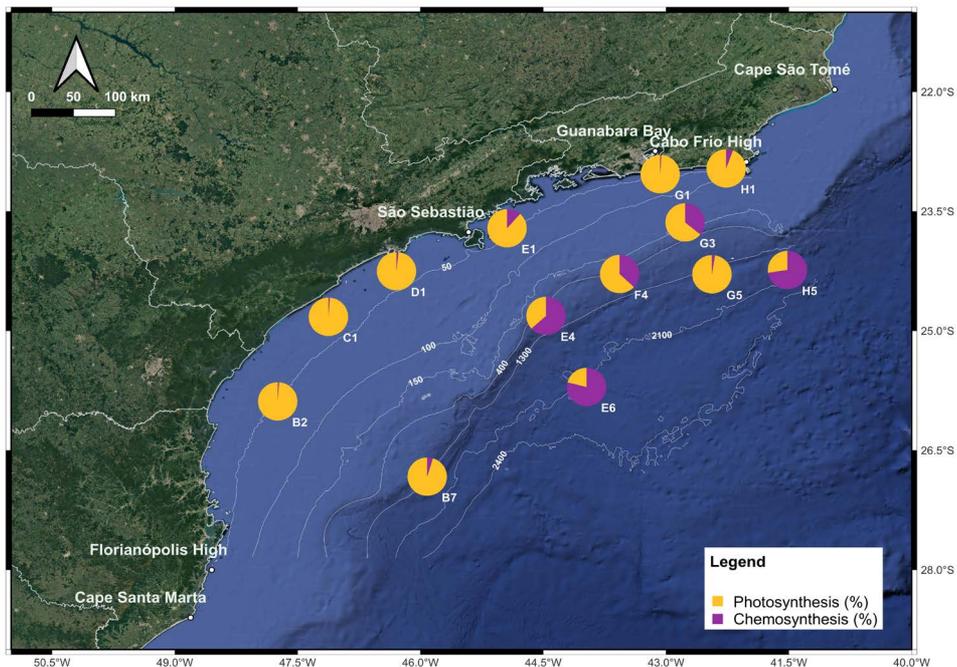
Figure 3. Relative importance (%) of photo- and chemosynthesis. Rates were integrated from the surface to the deep chlorophyll maximum (DCM), generating results in mg C m^{-2} h^{-1}.

We estimated the difference between surface and DCM temperatures to analyze possible effects on DCM rates incubated at surface temperature. Surface depths varied between 3 and 6 m, and the conservative temperature had mean and standard deviation equal to $21.93 \pm 1.61°C$. DCM varied between 10 and 139 m (average of 60 m) and was present in all 16 stations analyzed in this study. DCM's conservative temperature was approximately $20.87 \pm 1.55°C$. On average, the temperature difference between surface and DCM was 1.06°C, reaching a maximum value of 4.3°C. However, the median difference was 0.61°C, and the 75th percentile was 1.83°C, demonstrating that most values were below 2°C. Most stations (13/16) had surface and DCM depths in the same water mass (either CW or TW), indicating that environmental conditions were similar between layers. The difference in average temperature between surface ($T_2 = 21.93°C$ – incubation temperature) and DCM ($T_1 = 20.87°C$ – in situ temperature) enabled the estimation of the ratio $R_2/R_1 = 1.078$ for photosynthesis, which represents the possible increase in measured photosynthetic rates at the DCM (R_2) due to incubation at elevated temperatures. For chemosynthesis, the difference between incubation at room temperature ($T_2 = 22°C$) and average in situ DCM temperature ($T_1 = 20.87°C$) was equal to 1.13°C, resulting in $R_2/R_1 = 1.084$. In this way, the estimated increase in each productivity rate due to incubation in a higher temperature was, respectively, 7.8 and 8.4%. After dividing measured rates (R_2) by the ratios to encounter R_1 and performing a t-test between the two populations of normalized rates, the results showed no significant difference between means (p = 0.86 and 0.90, respectively), i.e., the reported DCM productivity rates were not significantly affected by incubation temperature.

Regarding abiotic variables, the nMDS corroborates the pattern of photosynthesis distribution (Figure 4A), with higher rates in the CW and MW at the bottom of the diagram and lower rates in the TW at the top of the diagram, forming a gradient that reflects underlying environmental variables on the dissimilarity matrix. Table S1 shows global statistics (mean, standard deviation, median, range, and number of observations) for all parameters. The PERMANOVA results indicated that the water masses significantly (p = 0.001) explained 84.3% of the variance in the ordination. PERMANOVA was also significant when dividing samples between pelagic zones ($R^2 = 0.67$, p = 0.001), layers ($R^2 = 0.84$, p = 0.001), and distance from the coastline ($R^2 = 0.38$, p = 0.001), but not between groups of transects ($R^2 = 0.08$, p = 0.08). As in previous analyses, we found no pattern of chemosynthesis distribution according to environmental variables, indicating that they were unable to explain its behavior (Figure 4B). We observed a clear separation of the pelagic zones, reflecting the physical and chemical variables used when plotting the ordination. However, chemosynthesis did not follow this arrangement.
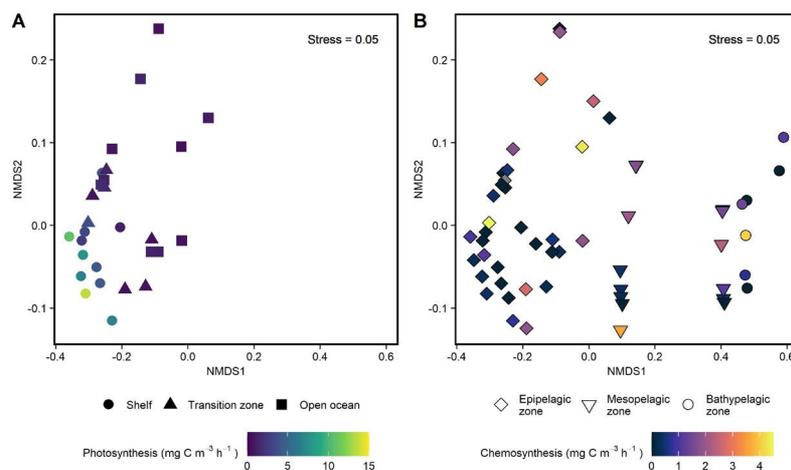

Figure 4. Non-Metric Multidimensional Scaling (nMDS) ordinations with photosynthetic (A; units in mg C m^{-3} h^{1}) and chemosynthetic (B; units in mg C m^{-3} h^{-1}) rates. Variables used were conservative temperature, absolute salinity, depth, mixed layer depth, dissolved oxygen, nitrite, nitrate, silicate, phosphate, turbidity, CDOM, chlorophyll-a, and phycoerythrin concentrations.

The winning model for predicting photosynthesis used CDOM, dissolved oxygen, and conservative temperature (R^2 = 0.76, p < 0.001). Since CDOM had five missing values, the final number of observations for the photosynthesis model was 23. During bootstrapping (n = 1,000), the predicted and observed values were tightly correlated (R^2 = 0.71) (Figure 5A). Figure 5B showed the linear regression between photosynthesis and CDOM, with the highest R^2 (R^2 = 0.66, p < 0.001) when considering all environmental variables. The relationship changed according to the water mass, increasing productivity and CDOM in the TW and decreasing productivity and increasing CDOM in the CW and MW. The association between CDOM and productivity

was preserved when considering surface and DCM separately ([Figure S2]). Dissolved oxygen and conservative temperature had very weak correlations to photosynthesis when considered by themselves (respectively, R^2 = 0.004, p = 0.36, and R^2 = 0.02, p = 0.21).

Although the same analytical effort was applied to predicting chemosynthesis, the predictive power of the variables was very low, as expected from the lack of patterns presented. The model used turbidity, phosphate, chlorophyll-a, and dissolved oxygen (R^2 = 0.17, p = 0.02) and had R^2 = 0.08 during bootstrapping (n = 1,000). The number of observations in the final model was 48 since turbidity had six missing values.
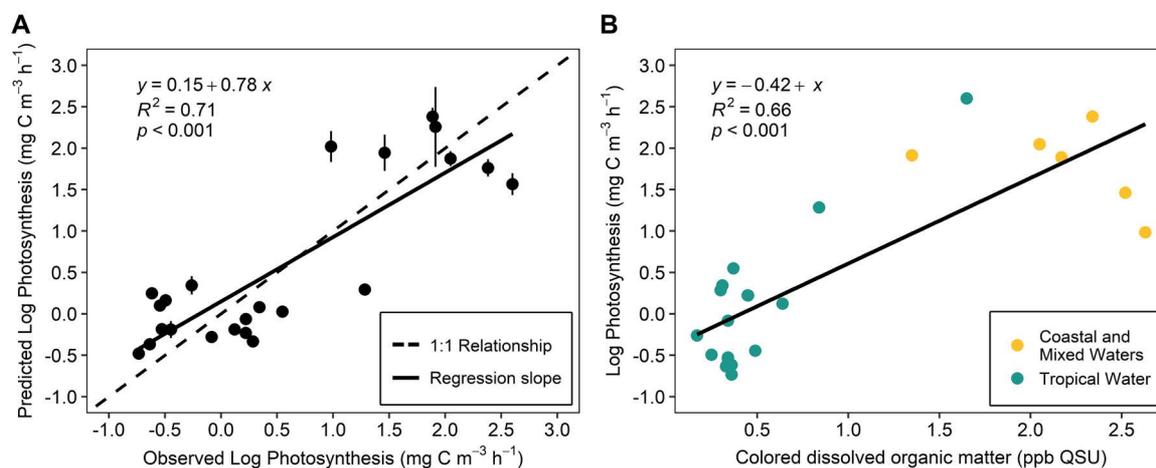

Figure 5. (A) Prediction of log photosynthesis by 1,000 iterations during bootstrapping. The dashed line represents the 1:1 relationship between observed and predicted values and the solid line represents the slope of the regression between them. The lines by each point represent the standard deviations of the predictions for the observation across all iterations. (B) Regression between log photosynthesis and colored dissolved organic matter (CDOM). Coastal and Mixed Water groups have the same color since means are statistically equal.

DISCUSSION

This study demonstrates that while photosynthesis has an established and more predictable behavior, chemosynthesis lacks patterns of distribution and predictability by the available environmental variables. Photosynthesis shows a clear oceanic-coastal gradient that goes along with CDOM concentrations and varies according to dominant community at each water mass. On the other hand, chemosynthesis presents unclear patterns of distribution and has great variability, indicating that it can be susceptible to

local oceanic phenomena. The former significantly predominated in most stations. However, the role of chemosynthesis is still substantial and can stand out according to environmental conditions.

PHOTOAUTOTROPHY

Photosynthetic rates are similar to previous results from *in situ* measurements in the region. Lutz et al. (2018) found an average of 2.94 ± 4.46 mg C m^{-3} h^{-1} for the winter period combining different studies. Brandini (1990a) measured photosynthesis between 0.01 and 8.09 mg C m^{-3} h^{-1}, with higher values corresponding to the

surface in coastal regions, decreasing towards the base of the euphotic zone.

Higher primary productivity in coastal waters compared to oceanic waters has also been reported in the area in other studies (e.g. Aidar-Aragão et al., 1980; Vieira and Teixeira, 1981; Brandini, 1990b). This gradient can be associated with more diverse light conditions, nutrients, phytoplankton composition, and grazing pressure on the shore (Lutz et al., 2018). Dunne et al. (2007) emphasized the importance of shelves (< 200 m deep) in the global carbon cycle, where 12% of total primary production and 85% of total burial flux occur. Furthermore, Longhurst et al. (1995) highlighted how coastal algal blooms are often influenced by a great number of processes, differently from oceanic algal blooms. Some may be river runoff, bathymetric features (e.g., seamounts, islands, shelf break, bottom roughness), tide and wind mixing, upwellings, and downwellings (Longhurst et al., 1995). During the cruise we came across the Plata River plume in coastal southern stations (Dottori et al., 2023), Agulhas rings downwelling (stations B7, E4, E6, E8, and H5), and Cabo Frio coastal upwelling (station H1; highest values following the surface of Guanabara Bay (Dottori et al., 2023)). Different biogeochemical fronts in the area have been described by Brandini et al. (2018).

The Guanabara Bay (GB) extreme outlier was expected. Guenther et al. (2008) measured surface rates as high as 48.5 μmol C L^{-1} h^{-1} (582 mg C m^{-3} h^{-1}) in the summer, and the surface mean during different tides varied from 8.78 to 20.3 μmol C L^{-1} h^{-1} (105.4 to 243.6 mg C m^{-3} h^{-1}). At the bottom station (20 m deep), without sunlight, the mean between tides varied from 0.20 to 0.38 μmol C L^{-1} h^{-1} (2.4 to 4.6 mg C m^{-3} h^{-1}). GB is a eutrophic and polluted coastal ecosystem, with high anthropogenic impact caused by rapid urban and industrial expansion (Villac and Tenenbaum, 2010). Furthermore, GB is the destination of considerable amounts of non-treated domestic and industrial wastes, increasing organic matter and nutrient concentrations in the water. These often favor auto- and heterotrophic production, resulting in (sometimes harmful) algal blooms (Villac and Tenenbaum, 2010; Aguiar et al., 2011; Signori et al., 2018). Lange et al. (2022) recently reported a succession of algal blooms between November and December of 2021 in beaches near GB. The authors associated these events with the intrusion of SACW, dragged by northeasterly winds that fertilize the surface, as described by Gonzalez-Rodriguez et al. (1992) and Gonzalez-Rodriguez (1994). The upwelling of the SACW in Cabo Frio was active during our cruise and affected the results at station H1.

The predominance of photosynthesis in the CW and MW compared to the TW mirrored the distribution of CDOM found in the region by Gonçalves-Araujo et al. (2019). The authors suggested that the significant correlation between CDOM and chlorophyll-a could indicate an autochthonous source of CDOM, a result of the shelf phytoplanktonic community dominated by diatoms (Brandini et al., 2014). Organelli and Claustre (2019) highlighted the importance of the picophytoplankton in shaping CDOM dynamics in the North Atlantic subtropical gyre, where *Synechococcus* and *Prochlorococcus* are substantial producers and increases in their abundances due to climate change can represent a rise in CDOM concentrations. These organisms have been reported in the Santos Basin, with higher concentrations in the warmer CW and colder TW, respectively, and with concentrations correlated with temperature (Bergo et al., 2017). Temperature has been highlighted as an important variable affecting microbial communities and processes in the South Atlantic Subtropical Gyre (Frazão et al., 2021). The lack of statistical significance between means of photosynthesis at surface and DCM (reported year-round in Santos Basin (Brandini et al., 2014)) may be associated with the presence of both layers in the same water mass in almost all stations. Furthermore, half of the sampling effort was during the winter, when gross primary production tends to decrease with increasing temperature (despite the fewer observations compared to the other seasons (Regaudie-de-Gioux and Duarte, 2012)). The relationship with dissolved oxygen, the last variable in the model, is more straightforward, as O_2 is one of the by-products of photosynthesis.

CHEMOAUTOTROPHY

Although the chemosynthetic rates in this study are the first that we are aware of in the spatial width of the Santos Basin, they are in the same order of

magnitude as those found in the South Atlantic by Prakash et al. (1991), which ranged from 0.17 to 3.81 mg C m^{-3} h^{-1}. Signori et al. (2018) measured dark carbon fixation from 0.001 to 2.72 mg C m^{-3} h^{-1} in GB, and Passos et al. (2022) reported rates between 0.02 and 0.3 mg C m^{-3} h^{-1} on the upper slope region of the basin. Farías et al. (2009) measured high rates in the upwelling off the Chilean coast, varying between 0.2 and 145 mg C m^{-3} d^{-1} (0.008 – 6.04 mg C m^{-3} h^{-1}) in the euphotic zone and between 0.16 and 117 mg C m^{-3} d^{-1} (0.007 – 4.87 mg C m^{-3} h^{-1}) in the aphotic zone. Other authors have found substantial rates in deep marine waters (Herndl et al., 2005; Reinthaler et al., 2010; Yakimov et al., 2014), even unrelated to oxic-anoxic interfaces, where conditions usually favor chemosynthesis due to the presence of a redox gradient that is independent of reduced carbon (Casamayor et al., 2001; Enrich-Prast et al., 2014).

Many factors can influence rate measurements during incubation experiments. Markager (1998) reported that the uptake of ^{14}C could be affected by incubation conditions and ineffective removal of inorganic carbon by HCl fuming. The author indicated that values higher than 10 µmol C m^{-3} h^{-1} (0.12 mg C m^{-3} h^{-1}) could be due to the release of nitrogen-rich compounds by planktonic cells damaged by agitation, pre-handling, and other incubation conditions during the experiment, which are particularly important in oligotrophic waters. Although Steemann-Nielsen (1952) recommended a 20 min HCl fumigation to remove inorganic carbon from the filter and Prakash et al. (1991) fumigated for 10 min, recent studies have fumigated for at least 12 h (Herndl et al., 2005; Yakimov et al., 2014). This is essential for low productivity systems where higher activities of ^{14}C are added to the samples, and residuals can constitute a larger fraction of the apparent dark assimilation (Markager, 1998). The limited fumigation time in our study may have overestimated rates due to the presence of inorganic carbon, though the added ^{14}C activity (5 µCi) was not as high as the 10 and 100 µCi added respectively by Yakimov et al. (2014) and Herndl et al. (2005).

Middelburg (2011) estimated that total dark carbon fixation on near-shore, shelf, slope, and open-ocean areas could be partitioned in 25, 17.5, 13.9, and 43.6%, respectively. However, rates in this study showed no significant difference when accounting for distance from the coastline. Chemosynthesis has also been reported to be higher and more variable in mesopelagic compared to bathypelagic zones (Reinthaler et al., 2010); however, the rates in this study were homogeneous between pelagic zones. Our results corroborate those of Li et al. (1993) for the North Atlantic and Sargasso Sea and of Passos et al. (2022) for the Santos Basin upper slope, where oceanic chemoautotrophy did not vary with depth. Farías et al. (2009) found that, on average, chemosynthetic production was divided equally in the euphotic and aphotic layers, suggesting that dark carbon fixation can be crucial in euphotic zones, the usual established realm of photosynthesis.

Based on other studies (Reinthaler et al., 2010; Zhou et al., 2017; Passos et al., 2022), the lack of association between dark carbon fixation and environmental parameters is common. Reinthaler et al. (2010) described that these relationships were weak but indicated that the large variability in the rates suggests the occurrence of "hotspots" of higher activity in the water column as opposed to a homogeneous ocean. The weak predictive model of chemosynthesis was composed of four variables: phosphate, chlorophyll-a, turbidity, and dissolved oxygen. Phosphate, a major macronutrient, is essential in energy storage and conversion, and in the synthesis of nucleic acids (DNA, RNA) and cell membrane phospholipids (Merchant and Helmann, 2012). The relationship with chlorophyll-a may be due to the need of electron donors (e.g., sulfide, ammonium, etc.) released in the water from the degradation of organic matter originally produced by photosynthesis (Enrich-Prast et al., 2014). Furthermore, organic matter in the water column increases turbidity. However, these correlations were weak, and we found no correlation between chemosynthesis and photosynthesis, which could be a hypothesis raised from these observations. The need for electron donors limits chemosynthesis, which could cause correlations between the process and ammonium, sulfur compounds (e.g., sulfate), methane, etc.; however, this study did not measured these. Dissolved oxygen is often the

main electron acceptor for aerobic chemosynthesis (Enrich-Prast et al., 2014).

RELATIVE IMPORTANCE OF MICROBIAL PROCESSES

Little is known about the percentage that chemosynthesis contributes to total primary production, especially in the Southwestern Atlantic Ocean. Nighttime dark carbon fixation can represent an increment of 2.5% (North Pacific) to 11% (Northwestern Atlantic) to total carbon fixation (Baltar and Herndl, 2019). Li et al. (1993) described a mean dark carbon fixation of 2% of the light carbon fixation at the surface and 10% at the DCM for the North Atlantic Ocean. Farías et al. (2009) and Signori et al. (2020) measured 20.3% and 36% of dark carbon fixation contribution in an upwelling system (off the coast of Chile) and in a lagoon off the coast of Brazil, respectively. Prakash et al. (1991) found higher ratios of dark and light ^{14}C uptake in the subtropical gyres and high southern latitudes (10 – 50%) compared to temperate and equatorial regions ($\leq$ 10%) and emphasized how variable the ^{14}C method for dark fixation can be. Thus, the 10.2% contribution of dark carbon fixation to total primary production that we found in the epipelagic zone of most stations is within the literature estimates and highlights an important role of chemosynthesis unaccounted for in global carbon budgets, as proposed by other authors (Middelburg, 2011; Baltar and Herndl, 2019).

Notably, we disregarded the excretion of dissolved organic carbon (DOC) by phytoplankton during incubation as a portion of unaccounted primary production. The only study that we are aware of on excretion of DOC in the Santos Basin was conducted by Vieira and Teixeira (1981), during the summer. They reported a variation of relative excretion rates between 2-30% (with 89% of values < 20%) of the total assimilated carbon in the incubation bottle, with higher percentages in low productivity areas (usually oligotrophic oceanic waters). Absolute excretion rates, however, varied with productivity rates. Low productivity areas (from 0 to 0.55 mg C m^{-3} h^{-1}) presented low excretion rates (average of 0.18 mg C m^{-3} h^{-1}, representing 20.2% of carbon assimilation). On the other hand, high productivity areas (> 20 mg C m^{-3} h^{-1}), such

as the Santos and Guanabara bays, had high excretion rates (average of 2.91 mg C m^{-3} h-1, representing only 3.1% of carbon assimilation). This corroborates descriptions by other authors: relative release of DOC is generally higher (40%, according to Fogg (1983)) in warm and oligotrophic waters such as the North Atlantic subtropical gyre during the summer, and lower (5% and 10-20%, according to Fogg (1983) and Thornton (2014), respectively) in nutrient-rich conditions, such as in coastal upwellings. Thus, excretion could have had an important effect in lowering photosynthetic rates in this study, especially in oceanic waters where productivity was significantly lower and excretion percentages are known to be higher. Furthermore, this could explain the peaking of relative chemosynthetic rates in oceanic regions, where photosynthesis could have been underestimated due to the loss in DOC.

Although proportions of photosynthesis and chemosynthesis may have been influenced by incubation period and conditions, excretion, and ineffective removal of inorganic carbon, most rates here observed are in line with the literature, except at stations E4, E6, and H5 where chemosynthesis surpassed photosynthesis. Besides the methodological reasons that could have affected our rate measurements, those stations were in regions affected by the Agulhas rings (Silveira et al., 2023), anticyclonic eddies that reach the South American boundary after shedding from the Agulhas Current (Guerra et al., 2018; Laxenaire et al., 2018). They had significant effects on the depression of isopycnals, extending oligotrophic waters to deeper regions and encompassing the whole epipelagic zone investigated. This could have influenced primary production, limiting photoautotrophs and enabling chemoautotrophs to prosper. However, knowledge on physical-biological coupling, especially for the latter, is scarce. Other studies integrating microbial processes with physical and chemical observations could be particularly necessary for oligotrophic waters, since environmental forcing has a substantial role in biological rates compared to trophic organization (Marañón et al., 2003) and few studies on dark carbon fixation have been conducted.

CONCLUSION

This study shows that photosynthesis has remained within the same order of magnitude in the region for the past four decades (Aidar-Aragão et al., 1980; Lutz et al., 2018; Brandini, 1990a). We contributed a new analysis that demonstrates the tight relationship between photosynthesis and CDOM, which has been previously explored by others by chlorophyll-a concentrations (Morel et al., 2010; Organelli and Claustre, 2019). Moreover, we showed that CDOM has significant predictive power, with higher rates and concentrations in the CW and lower in the TW. This distribution is also mirrored by phytoplankton communities such as *Synechococcus* and *Prochlorococcus* that have been linked to CDOM production in oligotrophic environments (Organelli and Claustre, 2019). On the other hand, chemosynthesis shows relative significance and susceptibility to environmental dynamics, although still with unclear patterns of behavior and predictability and apparently arbitrary hotspots of activity (as Reinthaler et al. (2010) pointed out for the dark ocean). Chemosynthesis represents 10.2% of total primary production in the Santos Basin; however, it can reach high values under different oceanographic scenarios. Further studies should investigate the effects of chemical and physical forcing on dark carbon fixation since it has accounted for more participation in the carbon cycle in recent research (e.g., Farías et al., 2009; Middelburg, 2011; Baltar and Herndl, 2019).

ACKNOWLEDGMENTS

AUTHOR CONTRIBUTIONS

D.S.K.: Conceptualization; Methodology; Formal analysis; Visualization; Writing – original draft; Writing – review & editing.

J.S.B.: Methodology; Formal analysis; Resources; Supervision; Writing – review & editing.

F.M.P.S.C.: Methodology; Resources; Writing – review & editing.

M.G.C.; P.M.T.: Methodology.

D.L.M.: Conceptualization; Resources; Supervision; Project Administration; Funding Acquisition; Writing – review & editing.

F.P.B.: Conceptualization; Methodology; Resources; Project Administration; Funding Acquisition; Writing – review & editing.

C.N.S.: Conceptualization; Methodology; Resources; Supervision; Project Administration; Funding Acquisition; Writing – review & editing.

REFERENCES

Aguiar, V., Neto, J. & Rangel, C. 2011. Eutrophication and hypoxia in four streams discharging in Guanabara Bay, RJ, Brazil, a case study. *Marine Pollution Bulletin*, *62*(8), 1915–1919. DOI: https://doi.org/10.1016/j.marpolbul.2011.04.035

Aidar-Aragão, E., Teixeira, C. & Vieira, A. 1980. Produção primária e concentração de clorofila-a na costa brasileira (Lat. 22º 31'S - Long. 41º52'W a Lat. 28º43'S - Long. 47º57'W). *Boletim Do Instituto Oceanográfico*, *29*(2), 9–14. DOI: https://doi.org/10.1590/s0373-55241980000200003

Baltar, F. & Herndl, G. 2019. Ideas and perspectives: Is dark carbon fixation relevant for oceanic primary production estimates? *Biogeosciences*, *16*(19), 3793–3799. DOI: https://doi.org/10.5194/bg-16-3793-2019

Bergo, N., Signori, C., Amado, A., Brandini, F. & Pellizari, V. 2017. The Partitioning of Carbon Biomass among the Pico- and Nano-plankton Community in the South Brazilian Bight during a Strong Summer Intrusion of South Atlantic Central Water. *Frontiers in Marine Science*, *4*, 238. DOI: https://doi.org/10.3389/fmars.2017.00238

Bird, R. E. & Hulstrom, R. L. 1981. *A Simplified Clear Sky Model for Direct and Diffuse Insolation on Horizontal Surfaces* (techreport No. SERI/TR-642-761). Golden: Solar Energy Research Institute.

Bowman, J., Kavanaugh, M., Doney, S. & Ducklow, H. 2018. Recurrent seascape units identify key ecological processes along the western Antarctic Peninsula. *Global Change Biology*, *24*(7), 3065–3078. DOI: https://doi.org/10.1111/gcb.14161

Brandini, F. 1990b. Hydrography and characteristics of the phytoplankton in shelf and oceanic waters off southeastern Brazil during winter (July/August 1982) and summer (February/March 1984). *Hydrobiologia*, *196*(2), 111–148. DOI: https://doi.org/10.1007/bf00006105

Brandini, F. 1990a. Produção primária e características fotossintéticas do fitoplâncton na região sueste do Brasil. *Brazilian Journal of Oceanography*, *38*(2), 147–159. DOI: https://doi.org/10.1590/s1679-87591990000200004

Brandini, F., Nogueira, M., Simião, M., Codina, J. & Noernberg, M. 2014. Deep chlorophyll maximum and plankton community response to oceanic bottom intrusions on the continental shelf in the South Brazilian Bight. *Continental Shelf Research*, *89*, 61–75. DOI: https://doi.org/10.1016/j.csr.2013.08.002

Brandini, F., Tura, P. & Santos, P. 2018. Ecosystem responses to biogeochemical fronts in the South Brazil Bight. *Progress in Oceanography*, *164*, 52–62. DOI: https://doi.org/10.1016/j.pocean.2018.04.012

Casamayor, E., García-Cantizano, J., Mas, J. & Pedrós-Alió, C. 2001. Primary production in estuarine oxic/anoxic interfaces: contribution of microbial dark CO_2 fixation in the Ebro River Salt Wedge Estuary. *Marine Ecology Progress Series*, *215*, 49–56. DOI: https://doi.org/10.3354/meps215049

Casamayor, E., García-Cantizano, J. & Pedrós-Alió, C. 2008. Carbon dioxide fixation in the dark by photosynthetic bacteria in sulfide-rich stratified lakes with oxic-anoxic interfaces. *Limnology and Oceanography*, *53*(4), 1193–1203. DOI: https://doi.org/10.4319/lo.2008.53.4.1193

Castro, B. 2014. Summer/winter stratification variability in the central part of the South Brazil Bight. *Continental Shelf Research*, *89*, 15–23. DOI: https://doi.org/10.1016/j.csr.2013.12.002

Crawley, M. J. 2015. *Statistics: an introduction using R* (2nd ed.). Sussex: John Wiley & Sons, Inc.

Dottori, M., Sasaki, D. K., Silva, D. A., Giovannino, S. R., Pinto, A. P., Gnamah, M., Santos, A. D., Silveira, I. C. A., Belo, W. C., Martins, R. P. & Moreira, D. L. 2023. Hydrographic structure of the continental shelf in Santos Basin and its causes: The SANAGU and SANSED campaigns (2019). *Ocean and Coastal Research*, *71*(Suppl 3).

Dunne, J., Sarmiento, J. & Gnanadesikan, A. 2007. A synthesis of global particle export from the surface ocean and cycling through the ocean interior and on the seafloor. *Global Biogeochemical Cycles*, *21*(4). DOI: https://doi.org/10.1029/2006gb002907

Enrich-Prast, A., Bastviken, D., Crill, P., Santoro, A., Signori, C. & Sanseverino, A. 2014. Reference Module in Earth Systems and Environmental Sciences. Elsevier. DOI: https://doi.org/10.1016/B978-0-12-409548-9.09054-0

Farías, L., Fernández, C., Faúndez, J., Cornejo, M. & Alcaman, M. 2009. Chemolithoautotrophic production mediating the cycling of the greenhouse gases N_2O and CH_4 in an upwelling ecosystem. *Biogeosciences*, *6*(12), 3053–3069. DOI: https://doi.org/10.5194/bg-6-3053-2009

Field, C., Behrenfeld, M., Randerson, J. & Falkowski, P. 1998. Primary Production of the Biosphere: Integrating Terrestrial and Oceanic Components. *Science*, *281*(5374), 237–240. DOI: https://doi.org/10.1126/science.281.5374.237

Fogg, G. 1983. The Ecological Significance of Extracellular Products of Phytoplankton Photosynthesis. *Botanica Marina*, *26*(1), 3–14. DOI: https://doi.org/10.1515/botm.1983.26.1.3

Fox, J. & Weisberg, S. 2019. *An R Companion to Applied Regression* (3rd ed.). Thousand Oaks: Sage. Accessed: https://socialsciences.mcmaster.ca/jfox/Books/Companion/

Frazão, L., Penninck, S., Michelazzo, L., Moreno, G., Guimarães, C., Lopes, R. & Signori, C. 2021. Microbial ecology of the South Atlantic Subtropical Gyre: a state-of-the-art review of an understudied ocean region. *Ocean and Coastal Research*, *69*. DOI: https://doi.org/10.1590/2675-2824069.20026lrf

Frouin, R. & Pinker, R. 1995. Estimating Photosynthetically Active Radiation (PAR) at the earth's surface from satellite observations. *Remote Sensing of Environment*, *51*(1), 98–107. DOI: https://doi.org/org/10.1016/0034-4257(94)00068-X

Gaeta, S. A. & Brandini, F. P. 2006. O Ambiente Oceanográfico da plataforma continental e do talude na região sudeste-sul do Brasil. *In*: Rossi-Wongtschowski, C. L. B. & Madureira, L. S. P. (eds.) (pp. 219–264). São Paulo: Edusp.

Gonçalves-Araujo, R., Röttgers, R., Haraguchi, L. & Brandini, F. 2019. Hydrography-Driven Variability of Optically Active Constituents of Water in the South Brazilian Bight: Biogeochemical Implications. *Frontiers in Marine Science*, *6*, 716. DOI: https://doi.org/10.3389/fmars.2019.00716

Gonzalez-Rodriguez, E. 1994. Yearly variation in primary productivity of marine phytoplankton from Cabo Frio (RJ, Brazil) region. *Hydrobiologia*, *294*(2), 145–156. DOI: https://doi.org/10.1007/bf00016855

Gonzalez-Rodriguez, E., Valentin, J., André, D. & Jacob, S. 1992. Upwelling and downwelling at Cabo Frio (Brazil): comparison of biomass and primary production responses. *Journal of Plankton Research*, *14*(2), 289–306. DOI: https://doi.org/10.1093/plankt/14.2.289

Grasshoff, K., Kremling, K. & Ehrhardt, M. 2009. *Methods of Seawater Analysis* (3rd ed.). Weinheim: Wiley-VCH.

Guenther, M., Paranhos, R., Rezende, C., Gonzalez-Rodriguez, E. & Valentin, J. 2008. Dynamics of bacterial carbon metabolism at the entrance of a tropical eutrophic bay influenced by tidal oscillation. *Aquatic Microbial Ecology*, *50*, 123–133. DOI: https://doi.org/10.3354/ame01154

Guerra, L., Paiva, A. & Chassignet, E. 2018. On the translation of Agulhas rings to the western South Atlantic Ocean. *Deep Sea Research Part I: Oceanographic Research Papers*, *139*, 104–113. DOI: https://doi.org/10.1016/j.dsr.2018.08.005

Guisan, A., Edwards, T. & Hastie, T. 2002. Generalized linear and generalized additive models in studies of species distributions: setting the scene. *Ecological Modelling*, *157*(2–3), 89–100.

Herndl, G. & Reinthaler, T. 2013. Microbial control of the dark end of the biological pump. *Nature Geoscience*, *6*(9), 718–724. DOI: https://doi.org/10.1038/ngeo1921

Herndl, G., Reinthaler, T., Teira, E., Van Aken, H., Veth, C., Pernthaler, A. & Pernthaler, J. 2005. Contribution of *Archaea* to Total Prokaryotic Production in the Deep Atlantic Ocean. *Applied and Environmental Microbiology*, *71*(5), 2303–2309. DOI: https://doi.org/10.1128/aem.71.5.2303-2309.2005

IOC, SCOR, & IAPSO. 2010. *The international thermodynamic equation of seawater – 2010: Calculation and use of thermodynamic properties* (56th ed.). London: UNESCO.

Karl, D. M. 2007. Microbial oceanography: paradigms, processes and promise. *Nature Reviews Microbiology*, *5*(10), 759–769. DOI: https://doi.org/10.1038/nrmicro1749

Kirchman, D. L. 2012. *Processes in microbial ecology*. Oxford: Oxford University Press.

Kirk, J. T. O. 2011. *Light and photosynthesis in aquatic ecosystems* (3rd ed.). Cambridge: Cambridge University Press.

Lange, P., Moser, G., Teixeira de Lima, D., Rodrigues, S., Fernandes, L. & S, N. 2022. An unprecedented harmful algae bloom on the beaches of Rio, Brazil. *Harmful Algae News (IOC-UNESCO)*, (70).

Laxenaire, R., Speich, S., Blanke, B., Chaigneau, A., Pegliasco, C. & Stegner, A. 2018. Anticyclonic Eddies Connecting the Western Boundaries of Indian and Atlantic Oceans. *Journal of Geophysical Research: Oceans*, *123*(11), 7651–7677. DOI: https://doi.org/10.1029/2018jc014270

Li, W. K. W., Irwin, B. D. & Dickie, P. M. 1993. Dark fixation of ^{14}C: Variations related to biomass and productivity of phytoplankton and bacteria. *Limnology and Oceanography*, *38*(3), 483–494. DOI: https://doi.org/10.4319/lo.1993.38.3.0483

Longhurst, A. & Harrison, W. 1989. The biological pump: Profiles of plankton production and consumption in the upper ocean. *Progress in Oceanography*, *22*(1), 47–123. DOI: https://doi.org/10.1016/0079-6611(89)90010-4

Longhurst, A., Sathyendranath, S., Platt, T. & Caverhill, C. 1995. An estimate of global primary production in the ocean from satellite radiometer data. *Journal of Plankton Research*, *17*(6), 1245–1271. DOI: https://doi.org/10.1093/plankt/17.6.1245

López-Urrutia, Á., San Martin, E., Harris, R. & Irigoien, X. 2006. Scaling the metabolic balance of the oceans. *Proceedings of the National Academy of Sciences*, *103*(23), 8739–8744. DOI: https://doi.org/10.1073/pnas.0601137103

Lutz, V., Segura, V., Dogliotti, A., Tavano, V., Brandini, F., Calliari, D., Ciotti, A., Villafañe, V., Schloss, I., Corrêa, F., Benavides, H. & Cantonnet, D. 2018. Overview on Primary Production in the Southwestern Atlantic. *In*: Hoffmeyer, M. S., Sabatini, M. E., Brandini, F. P., Calliari, D. L., & Santinelli, N. H. (eds.), *Plankton Ecology of the Southwestern Atlantic* (pp. 101–126). Cham: Springer International Publishing. DOI: https://doi.org/10.1007/978-3-319-77869-3_6

Marañón, E., Behrenfeld, M., González, N., Mouriño, B. & Zubkov, M. 2003. High variability of primary production in oligotrophic waters of the Atlantic Ocean: uncoupling from phytoplankton biomass and size structure. *Marine Ecology Progress Series*, *257*, 1–11. DOI: https://doi.org/10.3354/meps257001

Markager, S. 1998. Dark uptake of inorganic ^{14}C in oligotrophic oceanic waters. *Journal of Plankton Research*, *20*(9), 1813–1836. DOI: https://doi.org/10.1093/plankt/20.9.1813

Merchant, S. & Helmann, J. 2012. Elemental economy: microbial strategies for optimizing growth in the face of nutrient limitation. *Advances in Microbial Physiology*, *60*, 91–210. DOI: https://doi.org/org/10.1016/B978-0-12-398264-3.00002-4

Middelburg, J. 2011. Chemoautotrophy in the ocean. *Geophysical Research Letters*, *38*(24). DOI: https://doi.org/10.1029/2011gl049725

Moreira, D. L., Dalto, A. G., Figueiredo Jr, A. G., Valerio, A. M., Bonecker, A. C. T., Signori, C. N., Namiki, C., Sasaki, D. K., Pupo, D. V., Silva, D. A., Kutner, D. S., Duque-Castaño, D. C., Marcon, E. H., Gallotta, F. D. C., Paula, F. S., Gallucci, F., Roque, G. C. F., Campos, G. S., Fonseca, ..., G. & Souza, S. H. M. 2023. Multidisciplinary Scientific Cruises for Environmental Characterization in Santos Basin. *Ocean and Coastal Research, 71*(Suppl 3).

Moreira, J. L. P., Madeira, C. V., Gil, J. A. & Machado, M. A. P. 2007. Bacias Sedimentares Brasileiras: Cartas Estratigráficas - Bacia de Santos. *Boletim de Geociências Da Petrobras*, *15*(2), 531–549.

Morel, A. 1991. Light and marine photosynthesis: a spectral model with geochemical and climatological implications. *Progress in Oceanography*, *26*(3), 263–306. DOI: https://doi.org/org/10.1016/0079-6611(91)90004-6

Oksanen, J., Blanchet, F., Friendly, M., Kindt, R., Legendre, P., Mcglinn, D., Minchin, P., Hara, R., Simpson, G., Solymos, P., Stevens, M., Szoecs, E. & Wagner, H. 2020. vegan: Community Ecology Package. Accessed: https://CRAN.R-project.org/package=vegan

Organelli, E. & Claustre, H. 2019. Small Phytoplankton Shapes Colored Dissolved Organic Matter Dynamics in the North Atlantic Subtropical Gyre. *Geophysical Research Letters*, *46*(21), 12183–12191. DOI: https://doi.org/10.1029/2019gl084699

Passos, J. G., Soares, L. F., Sumida, P. Y. G., Bendia, A. G., Nakamura, F. M., Pellizari, V. H. & Signori, C. N. 2022. Contribution of chemoautotrophy and heterotrophy to the microbial carbon cycle in the Southwestern Atlantic Ocean. *Ocean and Coastal Research*, *70*(suppl 2). DOI: https://doi.org/10.1590/2675-2824070.22137jgp

Platt, T., Gallegos, C. L. & Harrison, W. G. 1980. Photoinhibition of photosynthesis in natural assemblages of marine phytoplankton. *Journal of Marine Research*, *38*, 687–701.

Poole, H. & Atkins, W. 1929. Photo-electric Measurements of Submarine Illumination throughout the Year. *Journal of the Marine Biological Association of the United Kingdom*, *16*(1), 297–324. DOI: https://doi.org/10.1017/s0025315400029829

Prakash, A., Sheldon, R. & Sutcliffe, W. 1991. Geographic variation of oceanic ^{14}C dark uptake. *Limnology and Oceanography*, *36*(1), 30–39. DOI: https://doi.org/10.4319/lo.1991.36.1.0030

R Core Team. 2021. A language and environment for statistical computing (Version 4.1.2). Accessed: https://www.R-project.org/

Regaudie-de-Gioux, A. & Duarte, C. M. 2012. Temperature dependence of planktonic metabolism in the ocean. *Global Biogeochemical Cycles*, *26*(1). DOI: https://doi.org/10.1029/2010GB003907

Reinthaler, T., Van Aken, H. & Herndl, G. 2010. Major contribution of autotrophy to microbial carbon cycling in the deep North Atlantic's interior. *Deep Sea Research Part II: Topical Studies in Oceanography*, *57*(16), 1572–1580. DOI: https://doi.org/10.1016/j.dsr2.2010.02.023

Schlitzer, R. 2021. Ocean Data View. Accessed: https://odv.awi.de/

Signori, C., Felizardo, J. & Enrich-Prast, A. 2020. Bacterial production prevails over photo- and chemosynthesis in a eutrophic tropical lagoon. *Estuarine, Coastal and Shelf Science*, *243*, 106889. DOI: https://doi.org/10.1016/j.ecss.2020.106889

Signori, C., Valentin, J., Pollery, R. & Enrich-Prast, A. 2018. Temporal Variability of Dark Carbon Fixation and Bacterial Production and Their Relation with Environmental Factors in a Tropical Estuarine System. *Estuaries and Coasts*, *41*(4), 1089–1101. DOI: https://doi.org/10.1007/s12237-017-0338-7

Silveira, I., Napolitano, D. & Farias, I. 2020. Water Masses and Oceanic Circulation of the Brazilian Continental Margin and Adjacent Abyssal Plain. *In*: Sumida, P. Y. G., Bernardino, A. F., & De Léo, F. C. (eds.) Brazilian Marine Biodiversity. (pp. 7–36). Berlim: Springer International Publishing. DOI: https://doi.org/10.1007/978-3-030-53222-2_2

Silveira, I. C. A., Lazaneo, C. Z., Amorim, J. P. M., Borges-Silva, M., Bernardo, P. S., Martins, R. C., Santos, D. M. C., Dottori, M., Belo, W. C., Martins, R. P. & Moreira, D. L. 2023. Oceanographic conditions of the continental slope and deep waters in Santos Basin: the SANSED cruise (winter 2019). *Ocean and Coastal Research*, *71*(suppl 3).

Sorokin, J. 1964. On the Trophic Role of Chemosynthesis in Water Bodies. *Internationale Revue Der Gesamten Hydrobiologie Und Hydrographie*, *49*(2), 307–324. DOI: https://doi.org/10.1002/iroh.19640490205

Steemann-Nielsen, E. 1952. The Use of Radio-active Carbon (C14) for Measuring Organic Production in the Sea. *ICES Journal of Marine Science*, *18*(2), 117–140. DOI: https://doi.org/10.1093/icesjms/18.2.117

Synergy Software. KaleidaGraph, Version 4.0 for Windows. Reading, PA, USA. Accessed: https://www.synergy.com/

Teixeira, C. 1973. Introdução aos métodos para medir a produção primária do fitoplâncton marinho. *Boletim Do Instituto Oceanográfico*, *22*(0), 59–92. DOI: https://doi.org/10.1590/s0373-55241973000100004

Thimijan, R. W. & Heins, R. D. 1983. Photometric, Radiometric, and Quantum Light Units of Measure: A Review of Procedures for Interconversion. *Hortscience*, *18*(6), 818–822.

Thornton, D. 2014. Dissolved organic matter (DOM) release by phytoplankton in the contemporary and future ocean. *European Journal of Phycology*, *49*(1), 20–46. DOI: https://doi.org/10.1080/09670262.2013.875596

Vicente, T., Yamashita, C., Sousa, S. & Ciotti, A. 2021. Evaluation of the relationship between biomass of living (stained) benthic foraminifera and particulate organic matter vertical flux in an oligotrophic region, Campos Basin, southeastern Brazilian continental margin. *Journal of Sea Research*, *176*, 102110. DOI: https://doi.org/10.1016/j.seares.2021.102110

Vieira, A. & Teixeira, C. 1981. Excreção de materia orgânica dissolvida por populações fitoplanctônicas da costa leste e sudeste do Brasil. *Boletim Do Instituto Oceanográfico*, *30*(1), 9–25. DOI: https://doi.org/10.1590/s0373-5524198100100003

Villac, M. & Tenenbaum, D. 2010. The phytoplankton of Guanabara Bay, Brazil: I. historical account of its biodiversity. *Biota Neotropica*, *10*(2), 271–293. DOI: https://doi.org/10.1590/s1676-06032010000200030

Welschmeyer, N. 1994. Fluorometric analysis of chlorophyll a in the presence of chlorophyll b and pheopigments. *Limnology and Oceanography*, *39*(8), 1985–1992. DOI: https://doi.org/10.4319/lo.1994.39.8.1985

Wickham, H. 2016. *ggplot2: Elegant Graphics for Data Analysis*. New York: Oxford University Press.

Yakimov, M., La Cono, V., Smedile, F., Crisafi, F., Arcadi, E., Leonardi, M., Decembrini, F., Catalfamo, M., Bargiela, R., Ferrer, M., Golyshin, P. & Giuliano, L. 2014. Heterotrophic bicarbonate assimilation is the main process of *de novo* organic carbon synthesis in hadal zone of the Hellenic Trench, the deepest part of Mediterranean Sea. *Environmental Microbiology Reports*, *6*(6), 709–722. DOI: https://doi.org/10.1111/1758-2229.12192

Zhou, W., Liao, J., Guo, Y., Yuan, X., Huang, H., Yuan, T. & Liu, S. 2017. High dark carbon fixation in the tropical South China Sea. *Continental Shelf Research*, *146*, 82–88. DOI: https://doi.org/10.1016/j.csr.2017.08.005